Molecular Biology of the Cell
Vol. 14, 642–657, February 2003

Microtubule Organization Requires Cell Cycle-dependent Nucleation at Dispersed Cytoplasmic Sites: Polar and Perinuclear Microtubule Organizing Centers in the Plant Pathogen *Ustilago maydis*

Anne Straube,* Marianne Brill,*† Berl R. Oakley,‡ Tetsuya Horio,§ and Gero Steinberg*‖

*Max-Planck-Institut für Terrestrische Mikrobiologie, Karl-von-Frisch-Straβe, D-35043 Marburg, Germany; ‡Departments of Molecular Genetics and Plant Biology, The Ohio State University, Columbus, Ohio 43210; and §Department of Food Microbiology, School of Medicine, University of Tokushima, Tokushima 770-8503, Japan

Submitted August 19, 2002; Revised October 19, 2002; Accepted October 31, 2002
Monitoring Editor: David Drubin

Growth of most eukaryotic cells requires directed transport along microtubules (MTs) that are nucleated at nuclear-associated microtubule organizing centers (MTOCs), such as the centrosome and the fungal spindle pole body (SPB). Herein, we show that the pathogenic fungus *Ustilago maydis* uses different MT nucleation sites to rearrange MTs during the cell cycle. In vivo observation of green fluorescent protein-MTs and MT plus-ends, tagged by a fluorescent EB1 homologue, provided evidence for antipolar MT orientation and dispersed cytoplasmic MT nucleating centers in unbudded cells. On budding γ-tubulin containing MTOCs formed at the bud neck, and MTs reorganized with >85% of all minus-ends being focused toward the growth region. Experimentally induced lateral budding resulted in MTs that curved out of the bud, again supporting the notion that polar growth requires polar MT nucleation. Depletion or overexpression of Tub2, the γ-tubulin from *U. maydis*, affected MT number in interphase cells. The SPB was inactive in G2 phase but continuously recruited γ-tubulin until it started to nucleate mitotic MTs. Taken together, our data suggest that MT reorganization in *U. maydis* depends on cell cycle-specific nucleation at dispersed cytoplasmic sites, at a polar MTOC and the SPB.

INTRODUCTION

The microtubule (MT) cytoskeleton is essential for various vital processes, including the assembly and function of the mitotic spindle, intracellular transport of organelles and vesicles, and the establishment and maintenance of cell polarity.

Article published online ahead of print. Mol. Biol. Cell 10.1091/mbc.E02–08–0513. Article and publication date are at www.molbiolcell.org/cgi/doi/10.1091/mbc.E02–08–0513.

† Present address: Institut für Medizinische Mikrobiologie, Immunologie und Hygiene, Trogerstraβe 4a, D-81675 München, Germany.

‖ Corresponding author. E-mail address: gero.steinberg@staff.uni-marburg.de.

Online version of this article contains video material for some figures. Online version available at www.molbiolcell.org.

Abbreviations used: CFP, cyan fluorescent protein; GFP, green fluorescent protein; MT, microtubulus; MTOC, microtubule organizing center; PTS, paired tubulin structures; SPB, spindle pole body; YFP, yellow fluorescent protein.

MTs are polymers composed of α- and β-tubulin heterodimers, which produce an inherent polarity in their structure and result in differences in their ends. MT-plus ends show dynamic instability behavior, characterized by the stochastic switching between phases of elongation and rapid shortening (Desai and Mitchison, 1997). Several proteins are known to interact preferentially with the plus end of MTs and are known to modify their stability. Among these are proteins of the EB1 family, which are conserved from yeast to humans (for review, see Tirnauer and Bierer, 2000) and localize to growing MT ends (Mimori-Kiyosue *et al.*, 2000). In contrast, MT minus ends are usually stabilized through contact with the perinuclear microtubule organizing center (MTOC), called the centrosome in vertebrates (Kirschner, 1978) and spindle pole body (SPB) in fungi (Heath, 1981). Both MTOCs contain γ-tubulin, a specialized tubulin isoform that was first identified in *Aspergillus nidulans* (Oakley and Oakley, 1989) and then found in a variety of eukaryotes (Joshi, 1994). γ-Tubulin is required for MT nucleation at the centrosome and the SPB (Oakley *et al.*, 1990;

Table 1. Strains and plasmids used in this study

Strains/plasmids	Genotype	Reference
FB1	*a1b1*	Banuett and Herskowitz, 1989
FB2	*a2b2*	Banuett and Herskowitz, 1989
521	*a1b1*	Banuett and Herskowitz, 1989
FB6a	*a2b1*	Banuett and Herskowitz, 1989
FB1rTub2	*a1b1 Pcrg-rub2, ble^R*	This study
FB1rTub2GT	*a1b1 Pcrg-tub2, ble^R* /potofGFPTub1	This study
FB1rTub2T2G	*a1b1 Pcrg-tub2,ble^R* /potofTub2GFP	This study
FB2T2G	*a2b2* /pcrgTub2GFP	This study
FB10T	*a1b1* /potefGFPTub1	Steinberg *et al.* 2001
FB2EBY	*a2b2 peb1-yfp, ble^R*	This study
FB2EBYCT	*a2b2 peb1-yfp, ble^R* /potefCFPTub1	This study
FB2rKin2GT	*a2b2 Pcrg-kin2, nar^R* /potefGFPTub1	This study
potefGFPTub1	*Potef-egfp-tub1, cbx^R*	Steinberg *et al.*, 2001
potefTub2GFP	*Potef-tub2-egfp, cbx^R*	This study
pcrgTub2GFP	*Pcrg-tub2-egfp, cbx^R*	This study
pCFPTub1	*Potef-cfp-tub1, hyg^R*	Wedlich-Soldner *et al.*, 2002

a, b, mating type genes; P, promoter; -, fusion; *ble^R*, phleomycine resistance; *nat^R*, nourseothricin resistance *cbx^R*, carboxin resistance; *hyg^R*, hygromycine resistance; /, ectopically integrated; *tub1, U. maydis* α-tubulin, *tub2, U. maydis* γ-tubulin; *peb1, U. maydis* EB1 homologue; *egfp,* enhanced green fluorescent protein; *yfp/cfp,* yellow-shifted/cyan-shifted fluorescent protein.

Horio *et al.*, 1991; Joshi *et al.*, 1992; Felix *et al.*, 1994). However, the mechanism by which it supports MT assembly is not resolved (Leguy *et al.*, 2000). Interestingly, in a variety of cells most MTs are not anchored at the centrosome and conclusively nonradial MT arrays are observed (Hyman and Karsenti, 1998). Different possibilities for the formation of noncentrosomal MTs have been proposed and experimentally proven. Free MTs are nucleated at, and released from, the centrosome (Keating *et al.*, 1997), or they can arise from MT breakage along their length (Waterman-Storer and Salmon, 1997) or by direct nucleation in the cytoplasm (Vorobjev *et al.*, 1997; Yvon and Wadsworth, 1997), which most likely involves cellular factors such as γ-tubulin. This is supported by the finding that γ-tubulin has been localized to putative noncentrosomal MTOCs (Horio *et al.*, 1991; McDonald *et al.*, 1993; Muresan *et al.*, 1993; Chabin-Brion *et al.*, 2001; Heitz *et al.*, 2001).

In this study, we use the basidiomycete fungus *Ustilago maydis* to expand our knowledge about how MT patterns can be generated. This dimorphic plant pathogen is amenable to molecular genetic and cytological methods and has proved to be an excellent model system for studying the role of motors and the cytoskeleton in polar growth and morphogenesis (Steinberg *et al.*, 2001; Straube *et al.*, 2001; Wedlich-Soldner *et al.*, 2002). Similar to *Saccharomyces cerevisiae*, haploid cells of *U. maydis* grow by polar budding (Banuett, 1995). However, the elongated cell shape and the existence of SPB-independent MTs, which are crucial for polar growth (Wedlich-Soldner *et al.*, 2000; Steinberg *et al.*, 2001; Wedlich-Soldner *et al.*, 2002), are reminiscent of fission yeast cells (Hagan, 1998). Thus, *U. maydis* combines features of both yeasts. Herein, we provide evidence for the existence of polar MTOCs that contain γ-tubulin and reorganize MTs at early budding in G2 phase, as suggested by in vivo observation of MT plus-ends, labeled with an EB1 homologue. In addition, in G1 and S phase multiple cytoplasmic MT nucleating centers nucleate MTs, whereas SPBs become active during mitosis. This is accompanied by a γ-tubulin rearrangement between the SPB and its cytoplasmic pool. Consistent with its assumed role in MT nucleation, γ-tubulin overexpression leads to more cytoplasmic MT tracks, whereas its depletion results in a drastic decrease in interphase MTs, mitotic defects and abnormal cell growth.

MATERIALS AND METHODS

Strains and Growth Conditions

U. maydis wild-type strains FB1 (*a1 b1*), FB2 (*a2 b2*), FB6a (*a2 b1*), and 521 (*a1 b1*) have been described previously (Banuett and Herskowitz, 1989; Table 1). Transformation was done as described previously (Schulz *et al.*, 1990). For FB2EBY, plasmid pPeb1YFP was integrated to the *peb1* locus of FB2 by homologous recombination. Strain FB1rTub2 contains plasmid pcrgTub2 homologous integrated into the *tub2* locus of FB1. Strain FB2T2G contains plasmid pcrgTub2GFP integrated into the succinate-dehydrogenase (*cbx*) locus (Keon *et al.*, 1991) of wild-type strain FB2. A plasmid containing green fluorescent protein (GFP)-α-tubulin (potefGFPTub1; Steinberg *et al.*, 2001) was integrated in the *cbx*-locus of FB1 and FB1rTub2, resulting in strains FB1GT and FB1rTub2GT, respectively. FB2EBYCT contains plasmid pCFPTub1 in the *cbx*-locus of strain FB2EBY. For strain FB2rKin2GT plasmid pcrgKin2 (Wedlich-Soldner, unpublished data) was integrated into the *kin2* locus of FB2GT (Steinberg *et al.*, 2001) by homologous recombination. To check for the functionality of the Tub2-GFP fusion protein we expressed the fusion construct under the constitutive *otef*-promoter (Spellig *et al.*, 1996; potefTub2GFP) in the conditional strain FB1rTub2, resulting in FB1rTub2T2G. Successful homologous recombination was confirmed by Southern blotting. Unless otherwise mentioned strains were grown overnight in complete medium (CM; Holliday, 1974) supplemented with 1% glucose (CM-G) or 1% arabinose (CM-A) at 28°C. Solid media contained 2% (wt/vol) bacto-agar. FB1rTub2 and FB1rTub2GT cells were grown over night in CM-A. One milliliter of the logarithmic growing culture was washed with 1 volume of CM-G, resuspended, and incubated in 10 ml of fresh CM-G at 28°C, 200 rpm. For late time points, a portion of these cells was incubated in fresh CM-G after 12–15 h of growth.

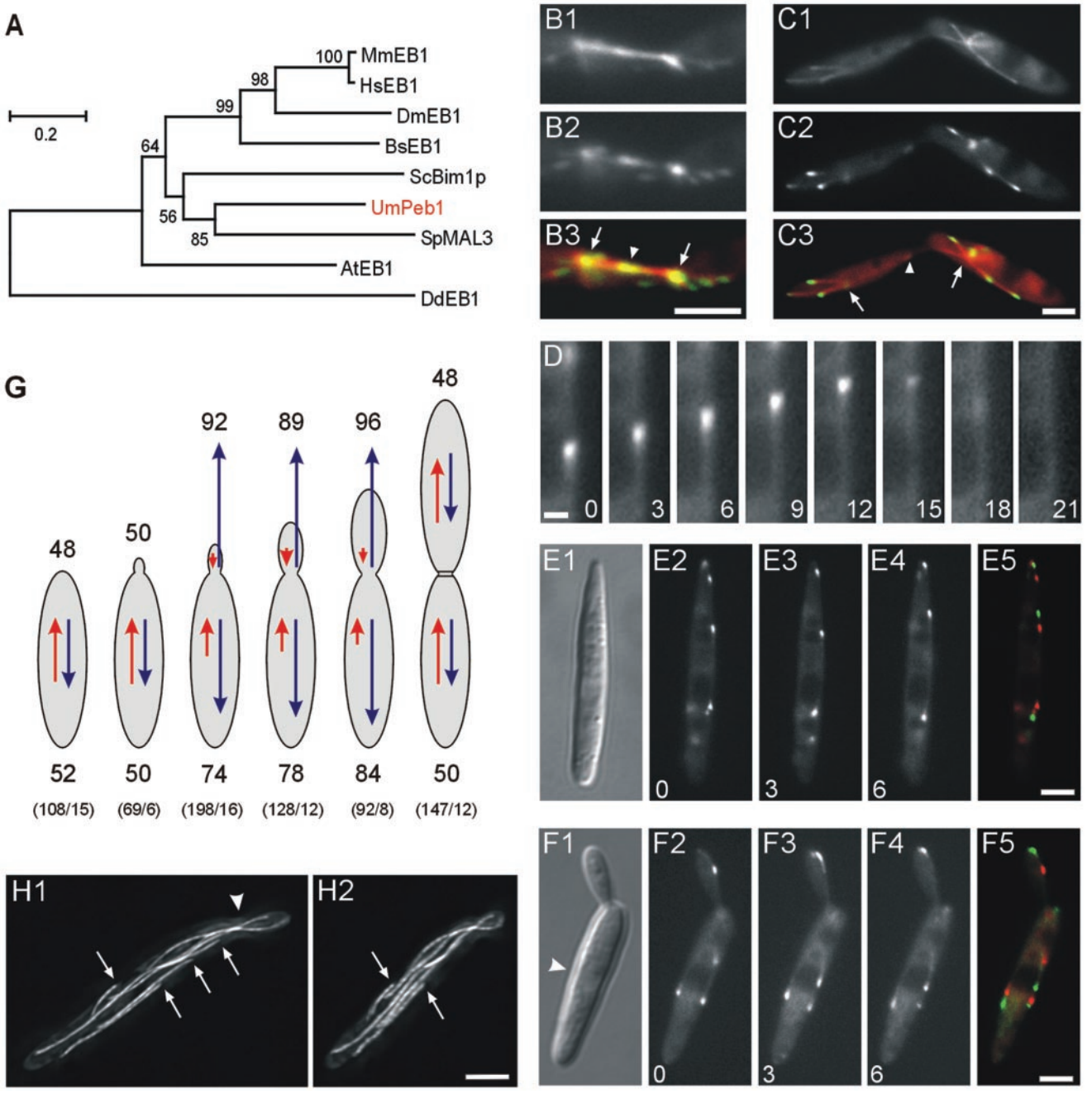

Figure 1. Peb1-YFP dynamics and MT orientation in *U. maydis*. (A) Phylogenetic tree of selected members of the EB1 family. Plus-end–binding protein Peb1 from *U. maydis* is closest related to MAL3 of *S. pombe*. Accession numbers for the used proteins are as follows: *Mus musculus* EB1, AAA96320; *Homo sapiens* EB1, I52726; *Drosophila melanogaster* EB1, AAF57390; *Botryllus schlosseri* EB1, CAA67697; *S. cerevisiae* Bim1p, NP010932; *U. maydis* Peb1, AJ489529; *S. pombe* MAL3, CAA70707; and *Arabidopsis thaliana* EB1, NP201056. Bootstrap values are given at the branching points. Bar, 0.2 substitutions per aa. (B and C) Peb1-YFP fusion protein (B2 and C2) localizes to the distal ends of MTs (CFP-Tub1; B1 and C1) as could clearly be seen during late anaphase (overlays in B3 and C3; CFP-Tub1 in red and Peb1-YFP in green). Note that Peb1-YFP localizes also to the midzone of the spindle (arrowheads in B3 and C3) and the spindle poles (arrows in B3 and C3). Bars, 3 μm. (D) Peb1-YFP localizes to growing ends of MTs. As soon as the MT starts shrinking, the Peb1-YFP signal disappears. Note that the MT is labeled by a faint Peb1-YFP signal. Time is given in seconds in the lower right corner. Bar, 1 μm. For movie, see supplementary material. (E and F) Motility of Peb1-YFP in an unbudded (E) and a budded cell (F). Peb1-YFP binds only to growing MT plus-ends and its motility indicates MT orientation. E5 and F5 show overlays of time points 0s (red) and 6s (green). Times between frames are given in seconds in the lower left corners. Bars, 3 μm. For movie, see supplementary material. (G) Quantification of MT orientation in interphase. Blue arrows and numbers above and below the cartoons are percent of Peb1-YFP dots moving to either tip of the cell. Red arrows show the relative amount

Isolation of tub2 and Plasmid Construction

The *tub2* gene was identified in a polymerase chain reaction (PCR) approach. This was done using genomic DNA of *U. maydis* and primers and protocols that were previously used to isolate γ-tubulin (Kube-Granderath and Schliwa, 1997). The obtained DNA fragment consisted of 543 base pairs and covered amino acid 179–360. All subsequent cloning was done using *Escherichia coli* K12 strain DH5α (Bethesda Research Laboratories, Gaithersburg, MD) following standard protocols (Sambrooke *et al.*, 1989). The PCR fragment was sequenced and used to identify a full-length clone in a cosmid library. Cosmid 1G4 was digested and a *Hin*dIII DNA fragment of 4.6 kb and a *Pst*I fragment of 3 kb contained the full-length *tub2* gene. These fragments were cloned into pUC18, resulting in pTub2*Hin*dIII and pTub2*Pst*I, and both strands were sequenced.

pPeb1YFP. The *peb1* coding sequence was amplified from genomic DNA of wild-type strain 521 with primers AS54 (TGGTTGCCATATGGGTGAATCACGTACGGAG) and AS55 (CGTACCATGGCGCCGAACATCTCATCCTCGTCCG), thereby generating an *Nde*I site at the start codon and an *Nco*I site instead of the stop codon. Primers were chosen according to the genomic sequence provided by the Bayer CropScience AG (Leverkusen, Germany). The PCR fragment was cloned into pCR2.1-TOPO (Invitrogen, Carlsbad, CA) and sequenced. Then 513 base pairs of the 3′-untranslated region were amplified with AS56 (GTTCTGCATGCGCGTACGTGCCGAATG) and AS57 (AGAATGAAGCTTCGCTCACTCACCAACATC) with an *Sph*I and a *Hin*dIII site at the ends. In a five-fragment ligation, the *peb1*-ORF, eGFP together with the *nos*-terminator as *Nco*I-*Bgl*II fragment, the phleomycin resistance cassette as *Bgl*II-*Sph*I fragment, and the 3′ untranslated region of *peb1* were cloned into pSL1180 (Pharmacia, Peapack, NJ) opened with *Hin*dIII and *Nde*I.

pcrgTub2GFP. The carboxy-terminal *tub2-GFP* fusion construct under control of the *crg*-promoter was generated in several steps. The open reading frame of *tub2* was amplified from pTub2*Hin*dIII by using *Pfu*-polymerase (Stratagene, La Jolla, CA) and the primers TubG5 (GCCATATGCCCAGGGAACTGATC) and TubG11.2 (GCACATGTTTGCTCCTAAATCGTCTGGCCTGGCC). This generated an *Nde*I site at the start codon and an *Afl*III site and a linker of three amino acids (GAN) at the 3′ end of *tub2*. This fragment was cloned into pCR2.1-TOPO and sequenced. *Tub2* contains an internal *Nde*I site; therefore, the gene was excised as *Nde*I-*Bgl*II and *Bgl*II-*Afl*III fragments. In a four-fragment ligation these DNA fragments were combined with the *crg*-promoter as a *Kpn*I-*Nde*I fragment of 3.6 kb and an *Nco*I-*Kpn*I fragment containing the carboxin resistance gene eGFP and the plasmid backbone.

potefTub2GFP. A DNA fragment containing *tub2-eGFP* followed by the *nos*-terminator was excised from pcrgTub2GFP by digestion with *Nde*I and *Eco*RI and cloned into pCU4 (Brachmann, unpublished data), which contains the *otef*-promoter (Spellig *et al.*, 1996) and a carboxin resistance cassette.

pcrgTub2. The 5′-untranslated region of *tub2* was amplified from pTub2*Pst*I by using primers rev24 (TTCACACAGGAAACAGCTATGACC) and AS TUBG1 (CTGGATCCAGTTGCGCTTGTTGGAG), thereby generating a *Bam*HI site at the 3′ end. The PCR fragment was cloned into pCR2.1-TOPO and sequenced. Digestion with *Pst*I and *Bam*HI resulted in a fragment of 599 base pairs. The phleomycin resistance cassette was excised using *Bam*HI and *Kpn*I. A fragment containing the *crg*-promoter fused to *tub2* was obtained after *Nco*I-*Kpn*I digest from pcrgTub2GFP. All fragments were ligated into pSL1180, which was opened with *Nco*I and *Pst*I.

potefGFPTub1. Plasmid construction is described elsewhere (Steinberg *et al.*, 2001). In brief, GFP was fused to the amino terminus of the complete *tub1* gene, encoding an essential α-tubulin from *U. maydis.* The fusion construct is expressed under the control of the constitutive *otef*-promoter (Spellig *et al.*, 1996).

Antibody Production

Anti-MIPA. Antisera were produced as described previously (Oakley *et al.*, 1990). Antibodies were affinity purified against a 6-histidine/Aspergillus γ-tubulin (*mipA*) fusion protein as described in Ovechkina and Oakley (2001), with the very minor modification that the sera were diluted in Tris-buffered saline before being added to the 6-histidine/γ-tubulin column. Specificity was tested by Western blotting and immunofluorescence microscopy in *A. nidulans*.

G9. Mouse monoclonal antibodies were raised against *Schizosaccharomyces pombe* γ-tubulin expressed in bacteria (Horio *et al.*, 1999). Full-length *S. pombe* γ-tubulin was expressed in *E. coli* K12 strain BL21 pLysS (Promega, Madison, WI), purified, and used for immunizing mice. Hybridoma cells were generated and screened for the clones producing anti-γ-tubulin antibodies following the standard procedures. Seventy-eight distinctive clones were isolated, named G1–78, and analyzed. The recognizing epitope of antibody produced by each clone was mapped by testing the reactivity of antibody by Western blotting to either full-length or truncated γ-tubulin of various species expressed either in *S. pombe* or *E. coli*.

Sequence Analyses

Protein sequences of fungal γ-tubulins and EB1 proteins from plants, vertebrates, and fungi were downloaded from PubMed (http://www.ncbi.nlm.nih.gov/entrez/query.fcgi) and aligned in ClustalX (Thompson *et al.*, 1997). Phylogenetic and molecular evolutionary analyses were conducted using MEGA version 2.1 (Kumar *et al.*, 2001). Phylogenetic dendrograms were constructed using the minimum evolution method with a nearest neighbor joining tree as starting point and 500 Bootstrap replicates. Further sequence analysis was done using COILS (http://www.ch.embnet.org/software/COILS_form.html; Lupas *et al.*, 1991).

Light Microscopy and Image Analysis

For in vivo observation, Peb1-YFP or GFP/CFP-α-tubulin–containing cells from logarithmically growing cultures were embedded in 1% prewarmed low melt agarose and immediately observed using an Axiophot microscope (Carl Zeiss, Jena, Germany). Epifluorescence was observed using standard fluorescein isothiocyanate, yellow fluorescent protein (YFP), cyan fluorescent protein (CFP), 4,6-diamidino-2-phenylindole, and rhodamine filter sets. A specific filter set (BP 470/20, FT 493, BP 505–530; Carl Zeiss) was used for detection of eGFP fluorescence in colocalization studies. All images were taken using a cooled charge-coupled device camera (C4742-95; Bridgewater, NJ). For quantification of Tub2-GFP all images were taken at 32% lamp intensity at the same exposure time. To determine the intensity at the SPB, regions were defined at highest magnification, and the integrated intensity within this region was measured with Im-

Figure 1 (cont). of movement toward the bud neck. Unbudded cells and cells with very small buds showed an equal distribution of MTs growing to both cell poles. A polarization suddenly occurred when bud size reached 15% of mother cell length. After septum formation, bipolar MT organization could be observed in mother and daughter cell. All numbers are based on 45-s observation of 6–16 cells (total number of signals and number of cells is given in brackets observed). (H) Side views at two different angles on GFP-labeled MTs in a budded cell of strain FB1GT. The bud neck is marked with an arrowhead in H1. Most MTs have contact with the bud neck, but several MTs with both ends visible exist in the mother cell. The proximal MT ends are marked with arrows. For movie, see supplementary material.

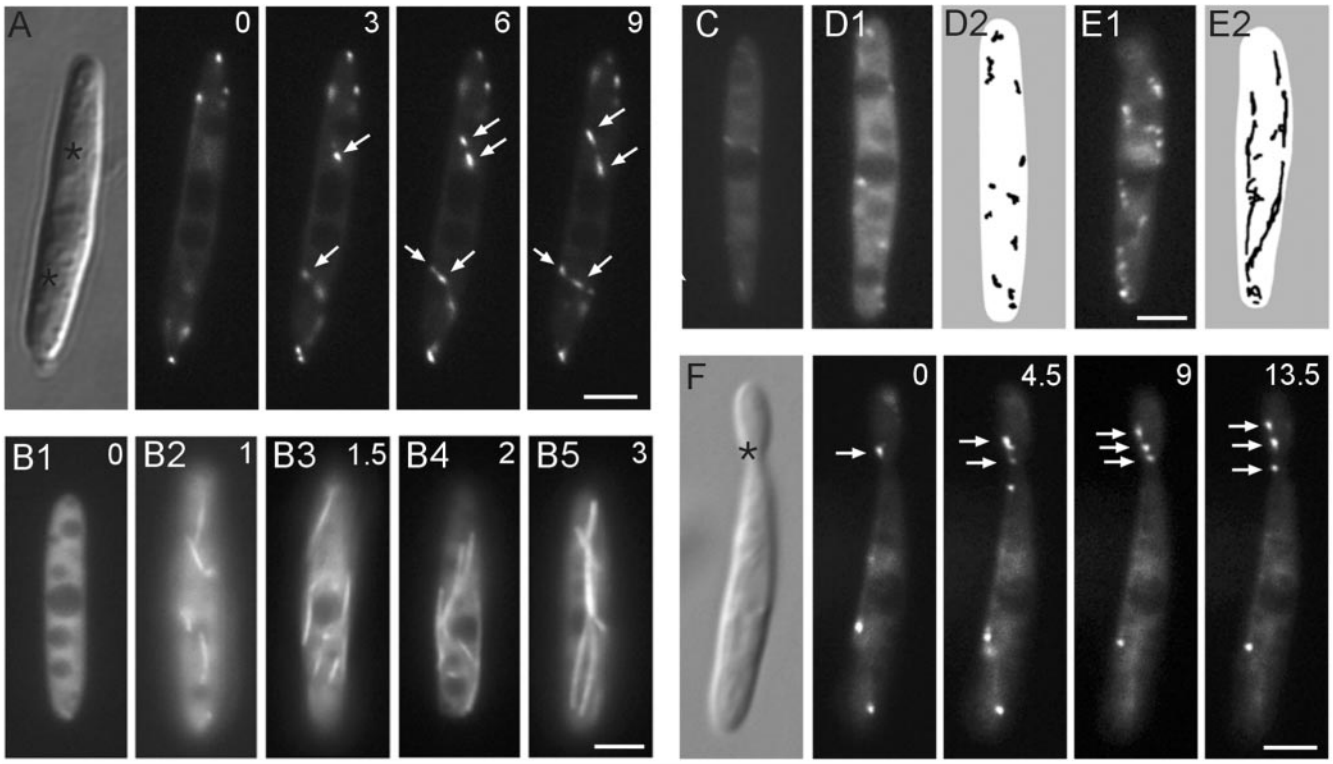

Figure 2. Sites of MT nucleation. (A) Nucleation sites were defined as sites where two or more Peb1-YFP signals (arrows) appeared at the same time and moved in different directions. Such nucleation sites were found randomly scattered within unbudded cells (asterisks in DIC image). Time between frames is given in seconds in the upper right corner. Bar, 3 μm. See videos in supplementary material. (B) No MTs could be detected anymore in FB1GT after benomyl treatment (B1). Nucleation of MTs started shortly after resuspending cells in fresh medium at several sites simultaneously (B2 and B3). MT growth (B3 and B4) was followed by its bundling (B5), and a normal MT pattern was reestablished within a few minutes of benomyl recovery. Time of recovery is given in minutes in the upper right corner. Bar, 3 μm. (C, D, and E) Only some faint Peb1-YFP signals resisted benomyl treatment (C). Bright Peb1-YFP dots reappeared 45 s after benomyl washout (D1) but moved never more than 1 μm in one direction as illustrated by tracking the movement of each Peb1-YFP signal (D2). Directed motion of Peb1-YFP dots (E) could be detected after 60-s recovery from benomyl treatment. Bar, 3 μm. For movie, see supplementary material. (F) In budded cells, multiple nucleation events are restricted to the neck region (asterisk in differential interference contrast image). Bar, 3 μm. See videos in supplementary material.

ageProPlus software (Media Cybernetics, Silver Spring, MD). The cytoplasmic Tub2-GFP background was determined as the average intensity of regions within the cytoplasm. Care was taken to exclude large organelles such as vacuoles, which would artificially reduce the measured intensity. The average image background was subtracted from the measured values. Timed movie stacks of FB2EBY cells were taken using ImageProPlus software and consisted of 30 frames with 1500-ms exposure time each. Peb1-YFP motion was tracked at the screen by following individual signals in all frames. Calculations and statistical analyses were performed using Excel (Microsoft, Redmond, WA) and PRISM (GraphPad Software, San Diego, CA). Image processing and measurements were done with ImageProPlus and Photoshop (Adobe Systems, Mountain View, CA). Deconvolution microscopy was done on imaging stacks that were generated by acquiring images at 500 ms with 60-nm step intervals by using a CoolSNAP-HQ charge-coupled device camera (Photometrics, Tucson, AZ) and a PiEFOC Piezo electric fast focus device (Physik Instrumente, Waldbronn, Germany), both controlled by the imaging software MetaMorph (Universal Imaging, Downingtown, PA). Image stacks were further processed using the deconvolution software AutoDeblur (AutoQuant, Watervliet, NY).

Immunolocalization and Staining Procedures

For indirect immunofluorescence of MTs, formaldehyde was added to growing cultures to a final concentration of 4% (EM-grade; Polysciences, Warrington, PA). Cells were fixed for 30 min, washed with phosphate-buffered saline (PBS) pH 7.2, and applied to coverslips that were precoated with poly-L-lysine (Sigma-Aldrich, St. Louis, MO). This was followed by several washes with PBS and 30 min of treatment with 3 mg/ml Novozyme (NovoNordisk, Bagsværd, Denmark) supplemented with Complete protease inhibitors (Roche Diagnostics, Indianapolis, IN). Subsequently, cells were washed and incubated in 0.3% Triton X-100 for 1 min, followed by additional washes and incubation in blocking reagent (1% milk in PBS) for 10 min. Anti-tubulin antibodies (from mouse; Oncogene Science, Cambridge, MA; and from rat, ImmunologicalsDirect, Oxfordshire, United Kingdom), anti-actin (Oncogene Science), MPM-2 (DAKO, Carpinteria, CA), anti-GFP (Bio-Cat, Heidelberg, Germany), and rhodamine-, Cy3-, and Cy2-conjugated secondary antibodies (Jackson Laboratories, West Grove, PA) were diluted in 0.2% milk, 0.01% azide in PBS and applied for 60 min. For colocalization studies with GFP fusion proteins, cells were fixed with 1–4% formaldehyde for 30 min and prepared for immunofluorescence as described above except that 0.2% Triton X-100 was applied for only 15 s.

Western Analysis

Western blotting was done according to standard protocols. Protein extracts were obtained by disruption of frozen *Ustilago* cells in mixer mill MM 200 (RETSCH, Haan, Germany) in 100 mM PIPES, pH 6.9, 5 mM $MgSO_4$, 1 mM EDTA, 5 mM EGTA supplemented with Complete protease inhibitor (Roche Diagnostics). Proteins were separated in 10% polyacrylamide gels and transferred onto nitrocellulose membranes for 30 min at 400 mA in a wet blot chamber. Antibody G9 was used 1:5000 to detect γ-tubulin according to standard procedures.

RESULTS

Peb1 Is a Member of the EB1 Family and Localizes to Microtubule Plus-Ends

To follow the growing MT plus-ends within MT bundles of *U. maydis* cells, we screened the genomic sequence of *U. maydis* (provided by the Bayer CropScience AG) for a member of the EB1 family of proteins that are known to bind to the dynamic plus-end of MTs (for review, see Tirnauer and Bierer, 2000). We found a gene, *peb1* (*p*lus *e*nd *b*inding) encoding for a putative protein of 289 amino acids (accession no. AJ489529). Peb1 shares 37% amino acid identity with its closest relative MAL3 from *S. pombe* (Beinhauer *et al.*, 1997; Figure 1A) and is a mildly acidic protein that contains a predicted coiled coil domain (aa 186 to 226) that is typical for EB1-like proteins. To check whether Peb1 indeed localizes to MT plus-ends, we constructed strain FB2EBYCT, which contained the YFP fused to the C terminus of the endogenous *peb1* gene and a cyan shifted fused to α-tubulin. Expression of both fusion proteins allowed the simultaneous observation of MTs and Peb1. We analyzed mitotic cells, in which the SPBs of *U. maydis* cells form MT asters with the minus ends associated with the SPB, whereas the MT plus-ends reach out into the cell (Steinberg *et al.*, 2001). In agreement with previous reports on the localization of EB1-like proteins in yeast and vertebrates (Berrueta *et al.*, 1998; Morrison *et al.*, 1998), Peb1-YFP was associated with the mitotic spindle and astral MTs (Figure 1B). Localization at plus ends was most obvious in late anaphase, when the plus ends of long astral MTs reached the cortex (Figure 1C). Colocalization with CFP-Tub1 during this stage revealed that all Peb1-YFP signals localized to MT tips or the SPBs (62 signals at 12 asters; arrows in Figure 1, B and C), where they might mark the ends of very short MTs. Peb1-YFP was also found in the midzone of the spindle, where, most likely, plus ends of overlapping MTs are located (arrowheads in Figure 1, B and C). Peb1-YFP stained exclusively growing MT ends, and the signal rapidly faded when MTs switched to shrinkage (Figure 1D). This behavior and localization pattern are characteristic for plus-end binding EB1 proteins (Morrison *et al.*, 1998; Tirnauer *et al.*, 1999; Mimori-Kiyosue *et al.*, 2000). Furthermore, Peb1-YFP signals moved slowly toward the cell poles in interphase (Figure 1, E and F). Their velocity was determined at 9.44 ± 0.89 μm/min (n = 12), which is not significantly different from the previously published elongation rate of GFP-MTs in *U. maydis* (P = 0.0731; Steinberg *et al.*, 2001). Taken together, our data strongly suggest that Peb1-YFP binds to growing MT plus-ends, and we therefore used it as an in vivo marker for the orientation of MTs.

Polar Growth Is Accompanied by a Change in MT Orientation

In vivo observation of Peb1-YFP allowed us to determine the orientation of MTs in different stages of the interphase. In unbudded cells and those with very small buds, motion of Peb1-YFP dots occurred toward both cell poles at equal frequency (Figure 1, E1–E4; overlay of E2 and E4 in 1E5; 1G, percentage of dots moving to either cell pole is indicated by the length of the arrows and is given in numbers). After the bud reached a size of ~15% of mother cell length, the MT cytoskeleton polarized with most of the MT plus ends growing away from the bud neck in both the mother and the daughter cell (1G). The polarization in the mother cell became more pronounced during later stages of bud growth (Figure 1, F and G). During these cell cycle stages the nucleus (arrowhead in Figure 1, F1) remained located within the mother cell and MT plus-ends passed it while growing to the distal cell pole (Figure 1F), suggesting that MTs are not nucleated at nuclear MTOCs. After mitosis, cells undergo cytokinesis and form two septa between mother and daughter cell. At this stage, MT elongation toward both poles of each cell was observed (Figure 1G). These data suggest that bud growth is accompanied by polar nucleation of MTs at the growth region, whereas unbudded and separated cells in G1 contain antipolar bundles. Interestingly, in budded cells only 85% of all MT polymerization was directed to the cell poles, indicating that not all MT minus ends are located at the neck region. This notion is supported by a three-dimensional reconstruction of the MT cytoskeleton labeled with GFP-Tub1 (Steinberg *et al.*, 2001) that clearly showed that mother cells contain short MTs that were not in contact with either the SPB or the neck region (Figure 1H, arrows mark proximal MT ends, arrowhead indicates the neck).

MT Nucleation Sites within Cytoplasm of Interphase Cells

In unbudded cells, Peb1-YFP signals suggested an antipolar orientation of MTs that were independent of the SPB. The Peb1-YFP signal rapidly faded when an MT underwent catastrophe and reappeared when an MT switched back to growth (Figure 1D). Because of this behavior, newly appearing Peb1-YFP signals should either represent such rescue events or indicate MT nucleation. Therefore, only the appearance of at least two Peb1-YFP dots at the same time and a certain location that moved in different directions is indicative of a nucleation event. We could not detect such nucleation events at the nucleus, indicating that the SPB is inactive during interphase. However, multiple nucleations occurred at random sites in unbudded cells (Figure 2A). To further confirm the existence of dispersed cytoplasmic MT-nucleating centers in unbudded cells, we disrupted MTs with benomyl and observed MT reappearance after washout of the drug. Treatment with 20 μM benomyl for 10 min was sufficient to fully depolymerize MTs in strain FB1GT and only an evenly distributed background of GFP-Tub1 remained (Figure 2B1). About 1 min after incubation in fresh medium, MTs started growing from numerous sites in the cell (Figure 2B2). Their number was determined with 6.5 ± 1.9 per focal plane of a cell (n = 34), and from this the total number of MTs per cell was estimated as 10–15. MT growth proceeded and was followed by bundling of MTs within the

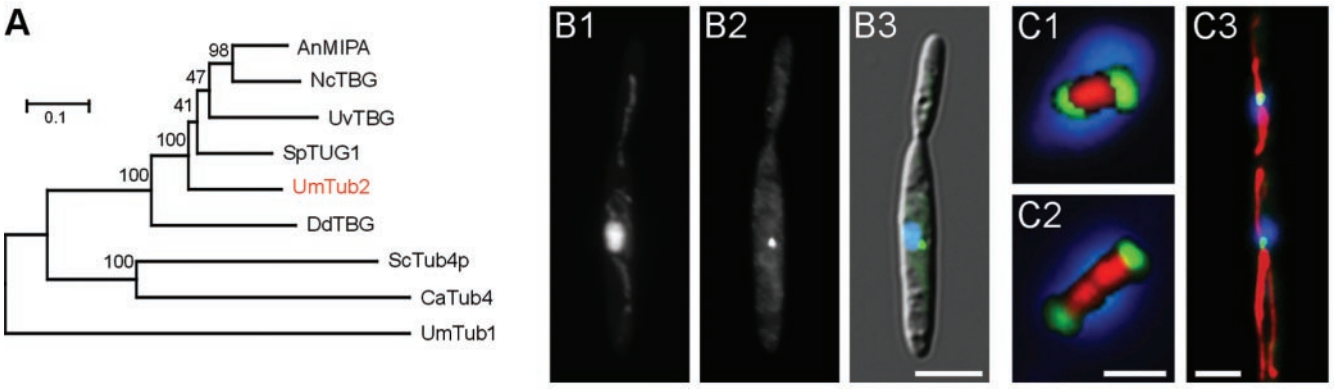

Figure 3. Localization of Tub2, the γ-tubulin of *U. maydis*, at the SPB. (A) Phylogenetic tree of fungal γ-tubulins. Tub1, the α-tubulin from *U. maydis*, was used as out-group. Tub2 is closest related to TUG1 from *S. pombe*. Accession numbers for the shown proteins are as follows: *A. nidulans* MIPA, P18695; *Neurospora crassa* GTUB, P53377; *Ustilago violacea* TBG, P32348; *S. pombe* TUG1, AAA35305; *U. maydis* Tub2, AJ489528; *Dictyostelium discoideum* TBG, CAA04130; *S. cerevisiae* Tub4p, P53378; and *U. maydis* Tub1, CAC17476. Bootstrap values are given at the branching points. Bar, 0.1 substitutions per aa. (B) Double staining of DNA (B1) and a Tub2-GFP fusion protein (B2). The overlay with a differential interference contrast image (B3) shows that Tub2-GFP (green) localizes to the nucleus (blue) that remains in the center of the mother cell during budding. Note that a high cytoplasmic background of Tub2-GFP is seen during interphase (B2). Bar, 5 μm. (C) Tub2-GFP localizes to the SPBs in metaphase (C1 and C2) and anaphase (C3; false colored overlays, DNA is given in blue, MTs in red, and Tub2-GFP in green). Bar for C1 and C2, 1 μm; and C3, 2 μm.

following 2 min (Figure 2B3–B5), finally resulting in a normal MT arrangement within only 5 min. Repeating this experiment with FB2EBY cells revealed that a minor population of Peb1-YFP signals were resistant to benomyl treatment (Figure 2C). However, these signals were faint and showed only Brownian motion. Many more bright Peb1-YFP-dots appeared 45 s after benomyl washout (Figure 2D1). These dots showed motility that was limited to an area <1 μm as could be seen by tracking the movement of each dot for 45 s during a timed movie stack (Figure 2D2). Furthermore, two or three dots appeared in most regions at least transiently during the observation time. This fits our criteria for MT nucleation events and argues for these regions being MT-nucleating centers. Directed motion of Peb1-YFP signals started after 60-s recovery from benomyl (Figure 2E). On the average 12.9 ± 2.1 ($n = 10$ cells) nucleating sites were evenly scattered within the focal plane of a cell at this time and 72% of these sites nucleated more than one MT. In summary, after benomyl treatment approximately half of the nucleation sites form MTs, and 10–15 MTs assemble to form the three to four MT bundles that were described previously (Steinberg *et al.*, 2001). In contrast to unbudded cells, Peb1-YFP motility in growing budded cells suggested the existence of polar MTOCs at the neck region. In agreement to this notion, multiple Peb1-YFP signals appeared at sites near the bud neck of small and medium size-budded cells (Figure 2F).

Tub2 Is the γ-Tubulin from U. maydis, Which Predominantly Localizes to SPB

To gain further evidence for cytoplasmic MTOCs, we attempted to visualize MTOCs by expressing a fusion protein of the γ-tubulin from *U. maydis* to GFP. We isolated *tub2*, the gene for γ-tubulin from *U. maydis* by using a PCR approach. The genomic sequence of *tub2* consists of 1538 base pairs, which encode a putative protein of 455 amino acids (accession no. AJ489528). Comparison of genomic and cDNA indicated that *tub2* contains two introns of 84- and 89-base pair length that are located 42 and 490 base pairs downstream of the start codon. Tub2 shares highest sequence identity with γ-tubulin from *S. pombe* (72%; Figure 3A). No additional γ-tubulin gene was detected in the genomic DNA of *U. maydis* by low-stringency Southern blotting (our unpublished data). For in vivo localization GFP was C-terminally fused to Tub2 and expressed under control of the inducible *crg*-promoter (Bottin *et al.*, 1996) in strain FB2T2G. Expression of Tub2-GFP had no influence on cell shape, growth on plates, and doubling time (FB2: 3.38 ± 0.14 h; FB2T2G: 3.30 ± 0.11; *t* test: not different, $P = 0.6739$; $\alpha = 0.05$, both grown in CM-A). The Tub2-GFP fusion protein localized to a single spot that was associated with the interphase nucleus as confirmed by 4,6-diamidino-2-phenylindole staining (Figure 3B, overlay of DNA in blue, Tub2-GFP in green, and Nomarski optics in 3B3). Before mitosis, the Tub2-GFP signal at the nucleus was duplicated and Tub2-GFP labeled the spindle poles during all stages of mitosis (Figure 3C, MTs in red, Tub2-GFP in green, and DNA in blue). This strongly argues that Tub2-GFP locates to the SPB during all stages of the cell cycle. Surprisingly, no specific Tub2-GFP signal was found in the neck region of budded cells and only a patchy cytoplasmic background was detected (Figures 3B2 and 8B). However, after amplification of the signal by using anti-GFP antibodies, we observed GFP-Tub2 at the neck region (see below; Figure 4, E and F), suggesting that the expected GFP-Tub2 at polar MTOCs was too faint to be detected.

Antibodies Against γ-Tubulin Detect Putative MTOCs at Bud Neck

Previous studies have shown that polar budding is accompanied by the appearance of two spherical tubulin structures at the growing cell pole that seem to bundle MT ends toward the growth region (Steinberg *et al.*, 2001). Therefore, we

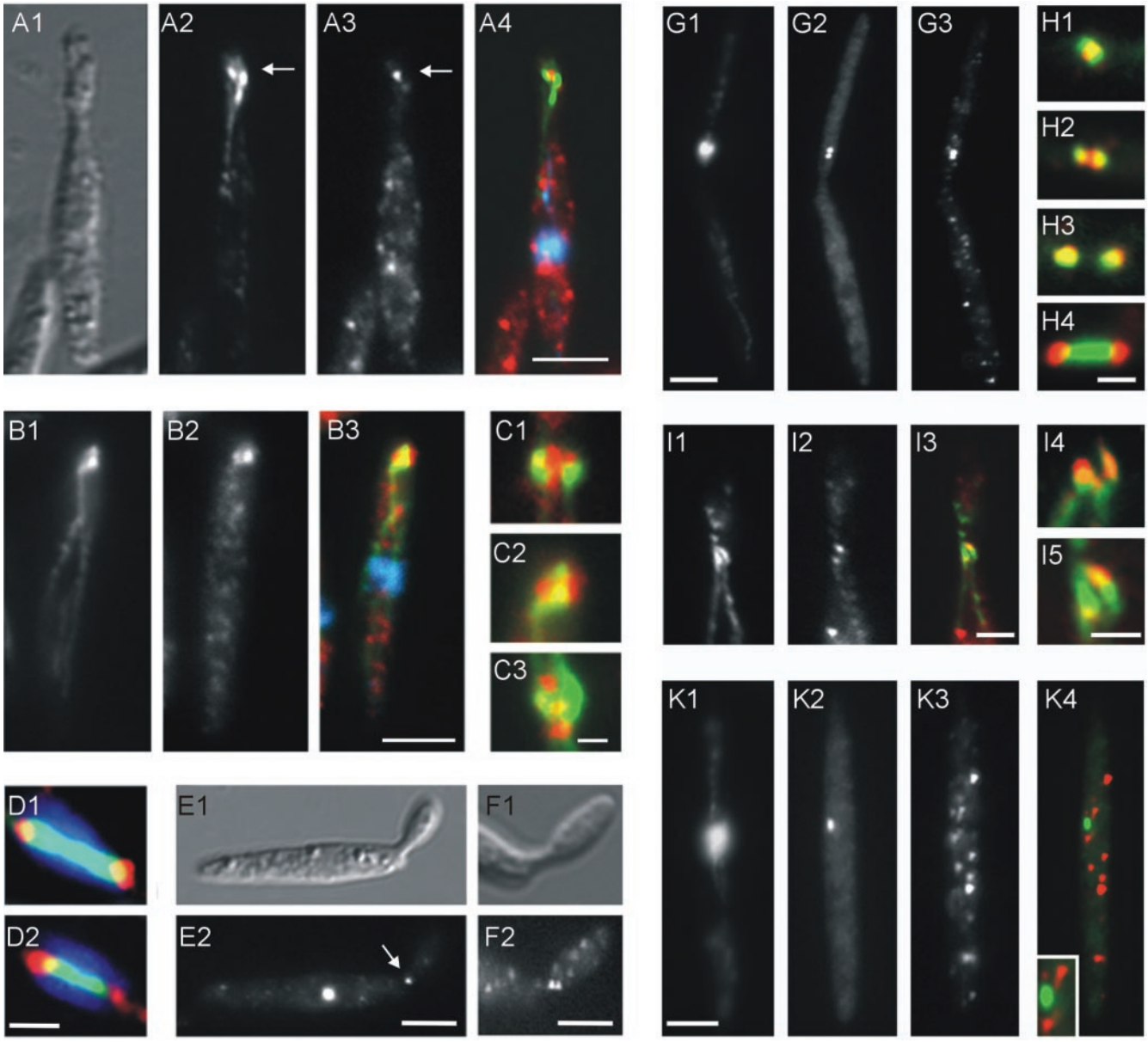

Figure 4. γ-Tubulin and MPM-2 antibodies decorate the PTS. (A) Cells with medium-sized buds (A1) contain PTS at the neck region that are labeled with tubulin antibodies (arrow in A2). In the same region a strong signal was detected using the G9 antibody (arrow in A3), indicating that γ-tubulin localizes to the PTS (A4, overlay of DNA in blue, tubulin in green, and γ-tubulin in red). Bar, 5 μm. (B) A polyclonal antibody against recombinant MIPA from *A. nidulans* also recognizes γ-tubulin (B2) at the PTS (B1, overlay in B3: DNA in blue, α-tubulin in green, and γ-tubulin in red. Bar, 5 μm. (C) Localization of anti MIPA (red) at the PTS (green) at higher magnification reveals that γ-tubulin localizes in between both tubulin spheres. Bar, 1 μm. (D) Staining of the spindle poles with antibodies G9 (D1) and anti-MIPA (D2) in FB1GT (DNA in blue, GFP-Tub1 in green, and γ-tubulin in red). Bar, 1 μm. (E and F) In situ localization of Tub2-GFP in cells of strain FB1rTub2T2G that was grown in CM-G. Under these conditions, the endogenous copy of Tub2 is repressed, whereas expression of Tub2-GFP fusion protein occurs (see Figure 7A). Anti-GFP antibodies recognize the SPB and a strong signal of Tub2-GFP in the neck (E1 and E2). Often a paired Tub2-GFP signal was detected in the neck region (F). Bars, 5 μm. (G) At the onset of mitosis, condensed DNA is located in the bud near the neck (G1). The SPBs labeled with Tub2-GFP (G2) separate while the spindle is formed. At this stage the SPBs have nucleation activity and the MPM-2 antibody clearly recognizes these active MTOCs (G3). Bar, 4 μm. (H) MPM-2 localization to mitotic SPBs at higher magnification. Tub2-GFP (green) and MPM-2 signals (red) colocalize (overlay results in yellow) at the beginning of SPB-separation (H1), and during spindle formation (H2) and elongation (H3). In mitotic cells of FB1GT the MPM-2 signal is located at the poles of the spindle (H4, anti MPM-2 in red; GFP-Tub1 in green). Bar, 1 μm. (I) The PTS (I1) often colocalized with MPM-2 reactive phosphoepitopes (I2), which are known to be components of active MTOCs (overlay in I3: α-tubulin in green, MPM-2 in red, and overlay results in yellow; higher magnification in given in I4 and I5). Bars, 2 μm in I1–I3, 1 μm in I4 and I5. (K) In interphase, the SPB contains the Tub2-GFP fusion protein (K2) and is closely associated with nuclear DNA (K1). At this stage the MPM-2 antibody gives a punctuate staining in the cytoplasm (K3), but does not recognize the SPB (false color overlay in K4, higher magnification of SPB region in inset), suggesting that the SPB is inactive. Bar, 3 μm.

considered it likely that these structures, named paired tubulin structures (PTS), coincided with the predicted polar MTOCs at the neck region. To support this assumption, we checked whether the PTS colocalize with γ-tubulin, which is an important component of MTOCs that supports MT nucleation (Oakley, 2000). The cross-reactive antibody G9 that was raised against bacterially expressed *S. pombe* γ-tubulin and whose epitope was mapped to the highly conserved region of γ-tubulin (Horio, unpublished observations) recognized a cytoplasmic background (Figure 4A3) and a single dot at the interphase nucleus (our unpublished data), which could be identified as the SPB in mitotic cells (Figure 4D1, false color overlay: DNA in blue, G9 in red, and spindle MTs in green). In addition, a polar γ-tubulin signal was found that colocalized with the PTS stained with anti-α-tubulin antibodies near the growth region (Figure 4A; false colored overlay in Figure 4A4: DNA in blue, G9 in red, and α-tubulin in green). A similar result was obtained using an antibody raised against MIPA from *A. nidulans*. A low cytoplasmic background and a strong signal at the PTS were obtained using the antibody at high dilution (Figure 4B, false colored overlay in Figure 4B3: anti-MIPA in red and α-tubulin in green), whereas higher concentrations were necessary to decorate the SPB in interphase (our unpublished data) and mitotic cells (Figure 4D2; DNA in blue, anti-MIPA in red, and spindle MTs in green). Higher magnification revealed that anti-MIPA often decorated two dispersed γ-tubulin signals localized between the spherical tubulin structures (Figure 4C; anti-MIPA in red, α-tubulin in green, and overlay results in yellow), where it might serve as a nucleation template and MT anchor. In addition, the PTS as the presumed main MTOC in budded cells could be detected with a GFP antibody in strain FB1rTub2T2G, where Tub2-GFP substituted for Tub2 (see below). Besides the SPB, one or two dots at the bud neck region are strongly labeled in that strain (Figure 4, E and F).

MPM-2 Recognizes Phosphoepitopes at Polar and Perinuclar MTOCs

To gain further evidence for the notion that the PTS are active MTOCs, we made use of the monoclonal antibody MPM-2 (Davis *et al.*, 1983) that recognizes phosphoepitopes, which are characteristic for active MTOCs in vertebrates, fungi, and plants (Centonze and Borisy, 1990; Masuda *et al.*, 1992; Vaughn and Harper, 1998). MPM-2 recognized the SPB of *U. maydis* in large-budded cells (Figure 4G3), when nuclei migrated in the proximal region of the bud (Figure 4G1) and the SPBs separated (Figure 4G2). The strong MPM-2 signal colocalizes with Tub2-GFP during all stages of mitosis (Figure 4H1–3; Tub2-GFP in green and MPM-2 in red) and detected the spindle poles in FB1GT cells (4H4; MTs in green and MPM-2 in red). Furthermore, we detected MPM-2–reactive phosphoepitopes at the PTS (Figure 4I; MPM-2 in red, α-tubulin in green, and overlay results in yellow in 4I3-I5), again suggesting that these structures are involved in MT nucleation during bud growth. We therefore conclude that MPM-2 detects active MTOCs in *U. maydis*. In unbudded cells, the nucleus is positioned in the cell center (Figure 4K1) and the associated SPB could be detected by Tub2-GFP (Figure 4K2). Although MPM-2 recognized several cellular components (Figure 4K3), the antibody did not label the SPB at this cell cycle stage (overlay in Figure 4K4; MPM-2 in red and Tub2-GFP in green). This argues for the SPB being inactive during interphase in *U. maydis* and coincides with the finding of cytoplasmic MT nucleation sites.

Lateral Budding in a Kinesin Mutant Leads to Bent MTs

Haploid *U. maydis* cells elongate and grow exclusively by polar budding (Wedlich-Soldner *et al.*, 2002). One might argue that MTs orient along the long axis due to their stiffness and reach the growth region by a stochastic chance mechanism. However, our data strongly indicate that polar MTOCs organize MTs during budding. Therefore, we predicted that laterally formed buds would contain MTOCs, too, and that MTs would bend out of the growing bud, thereby working against their physical stiffness. Lateral budding could never be observed in wild-type cells ($n > 1000$ cells). However, in strain FB2rKin2GT, in which the conventional kinesin Kin2 is ~200 times overexpressed in CM-A (Straube and Steinberg, unpublished data), lateral buds can be found in ~1% of the cells. These buds had normal size and shape and contained polar localized actin patches (Figure 5A) and PTS (Figure 5A2, inset), indicating that they are actively growing. In accordance with our prediction, MTs emanate from the PTS and bend out of the bud (Figure 5, B and C). Interestingly, MTs do not reach into very early buds (Figure 5D). This is in agreement to the finding that small buds are formed before MTs reorganization occurs (see above; Figure 1G), suggesting that that MTs are of less importance for early stages of budding. However, our data argue that polar cytoplasmic MTOCs organize MTs toward the growth region during budding of *U. maydis*.

The Number of MTs Depends on Tub2 Protein Level

Our localization data strongly indicated that Tub2 participates in the nucleation of MTs in *U. maydis*. To confirm this conclusion, we placed the endogenous *tub2* gene under control of the *crg*-promoter that allows a controlled expression depending on the carbon source (Bottin *et al.*, 1996). In this strain, FB1rTub2, Tub2 was overexpressed twofold at permissive conditions (CM-A), whereas the protein level decreased after shift to restrictive conditions (CM-G), and after 4 h in CM-G only traces of Tub2 could be detected on Western blots (Figure 6A). Residual amounts of Tub2 are most likely due to the incomplete repression of the used promoter and were not reduced after further incubation in CM-G (our unpublished data). Growth of FB1rTub2 was abolished on CM-G-plates, indicating that *tub2* is an essential gene (Figure 6B2).

To ascertain whether the Tub2-GFP fusion protein is biologically active we expressed the construct in the conditional mutant strain FB1rTub2 under control of the constitutive *otef*-promoter (Spellig *et al.*, 1996; strain FB1rTub2T2G). Under restrictive conditions the *tub2* gene was repressed but Tub2-GFP expression was increased (Figure 6A, right). This allowed growth of the conditional mutant strain on CM-G containing plates (Figure 6B3), suggesting that the fusion protein is active and can complement for the absence of endogenous γ-tubulin. Localization of Tub2-GFP fusion protein in the rescued strain was essentially the same as in FB2T2G, but amplifying the signal with an anti-GFP antibody made the polar MTOCs detectable (see above; Figure 4,

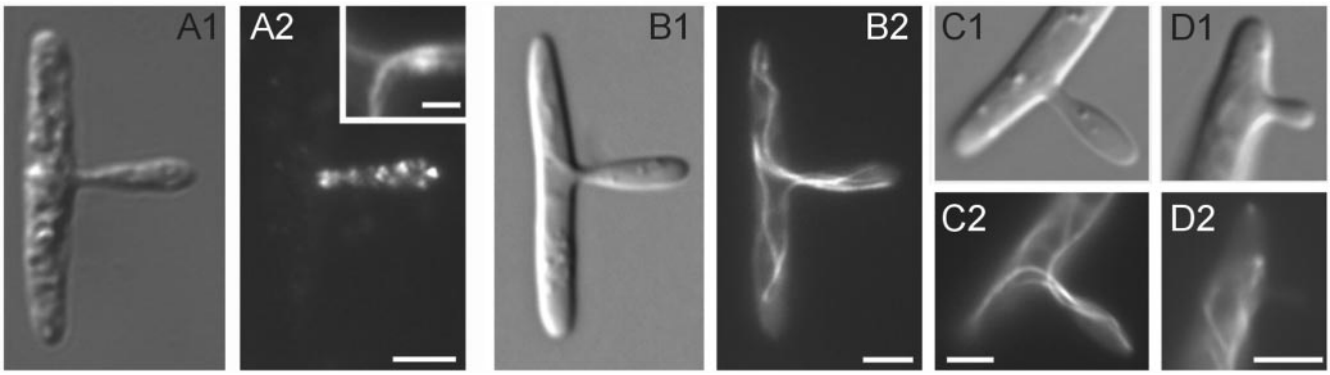

Figure 5. MT organization in lateral budding cells of a kinesin mutant FB2rKin2. (A) In situ localization of actin patches in the lateral bud (A1 and A2) indicates that the bud is actively growing. In agreement with the MT organization of control cells, paired tubulin structures are located in the bud near the neck region (inset in A2). Therefore, these structures are typical for growing buds, irrespective of the site of bud growth. Bar, 3 μm; inset in A2, 1 μm. (B–D) Overexpression of Kin2 occurs in strain FB2rKin2GT when grown in CM-A. This resulted in 1% cells that show lateral budding. In these cells, GFP-MTs bend to reach out of the bud into the mother cell (B2 and C2). Interestingly, small buds do not contain MTs (D1 and D2). Bars, 3 μm.

E and F). This confirmed the localization data obtained by using cross-reactive γ-tubulin antibodies.

Twofold overexpression of Tub2 in strain FB1rTub2 had no influence on cell growth (Figure 6B1) but affected the number of nucleated MTs. Immunofluorescence of wild-type FB1 cells with α-tubulin antibodies stained the PTS in the bud neck region (Figure 6C1). FB1rTub2 cells grown in CM-A showed larger PTS with an irregular distance between the two spherical tubulin structures and much brighter stained MTs within the bud (Figure 6C2 and C3, insets). Furthermore, Tub2 overexpression led to an increased number of MT tracks, which became obvious in optical cross sections of strains FB1rTub2GT and FB1GT, where MTs were labeled with GFP-Tub1 (Figure 6D1; MT tracks per cell: FB1GT, 3.38 $\pm$ 1.17, n = 62; Figure 6D2; FB1rTub2GT, 4.22 $\pm$ 1.04, n = 54; different, $P < 0.0001$). In both strains MT bundles were observed in 80% of the observed cells, indicating that the elevated number of MT tracks is due to an increased nucleating activity rather than splitting of MT bundles. Accordingly, depletion of Tub2 in FB1rTub2GT after 4 h under restrictive conditions led to a clear decrease in the number and length of interphase MTs (Figure 6E1–E3), although MTs did not completely disappear even after 23 h in CM-G (Figure 6F). Consistent with a role of γ-tubulin in organizing spindle MTs, many large-budded cells accumulated in the culture, which were often arrested in mitosis (Figure 6, E3 and F). In addition, with time in CM-G an increasing number of nonmitotic cells with aberrant and elongated morphology accumulated (Figure 6F).

Tub2-GFP Fusion Protein Is Gradually Recruited from Cytoplasm to SPBs

Monitoring the amount of Tub2-GFP fusion protein at the SPB relative to the cytoplasm revealed a dynamic rearrangement of γ-tubulin during the cell cycle. The intensity of the Tub2-GFP signal at the SPBs continuously increased during bud growth (Figure 7A; intensity is given in pseudocolours: blue, strong signal; red, weak signal; images correspond to cell cycle stages depicted in Figure 7C). We quantified this phenomenon by measuring the relative amount of Tub2-GFP signals at SPBs and in the cytoplasm based on digital images taken under exactly the same conditions (Figure 7B; measured region indicated by dashed line). In unbudded cells, which are most likely in late G1 or S phase (Snetselaar and McCann, 1997), the SPB-bound Tub2-GFP signal was weakest, whereas cytoplasmic staining was relatively strong (Figure 7C, values for Tub2-GFP intensity at SPB and in cytoplasm at this stages was set to 100%). During bud growth, the amount of Tub2-GFP fusion protein at the SPB gradually increased, whereas the cytoplasmic signal showed a reciprocal behavior, suggesting that Tub2-GFP fusion protein is recruited from the cytoplasm to SPB. Maximum intensity of the Tub2-GFP signal at the SPB was achieved in late G2 when nuclear migration into the bud occurred. The Tub2-GFP signal remained constant during mitosis (dashed bar in Figure 7C represents combined Tub2-GFP signals of pairs of mitotic SPBs). After nuclear division, the Tub2-GFP signal at the SPB decreased, whereas the amount of cytoplasmic Tub2-GFP slightly increased. This was followed by a rise of cytoplasmic staining in unbudded cells. These observations suggest that γ-tubulin is gradually recruited from the cytoplasm to the SPB during bud growth in G2, until both SPBs separate and become active in mitosis. The γ-tubulin cycling and the high cytoplasmic level of Tub2-GFP in interphase cells indicate a γ-tubulin–dependent nucleating activity in the cytoplasm.

DISCUSSION

Polar growth and morphological changes require the dynamic reorganization of the cytoskeleton followed by directed membrane traffic along filamentous actin and microtubules (Nabi, 1999). Recently, we demonstrated that MTs are involved in polar bud formation in *U. maydis* (Steinberg *et al.*, 2001). Dynein-mediated endosome transport is a crucial requirement for polar bud growth (Wedlich-Soldner *et al.*, 2000, 2002), suggesting that MT minus-ends are focused at the growing cell pole. Interestingly, SPB-independent

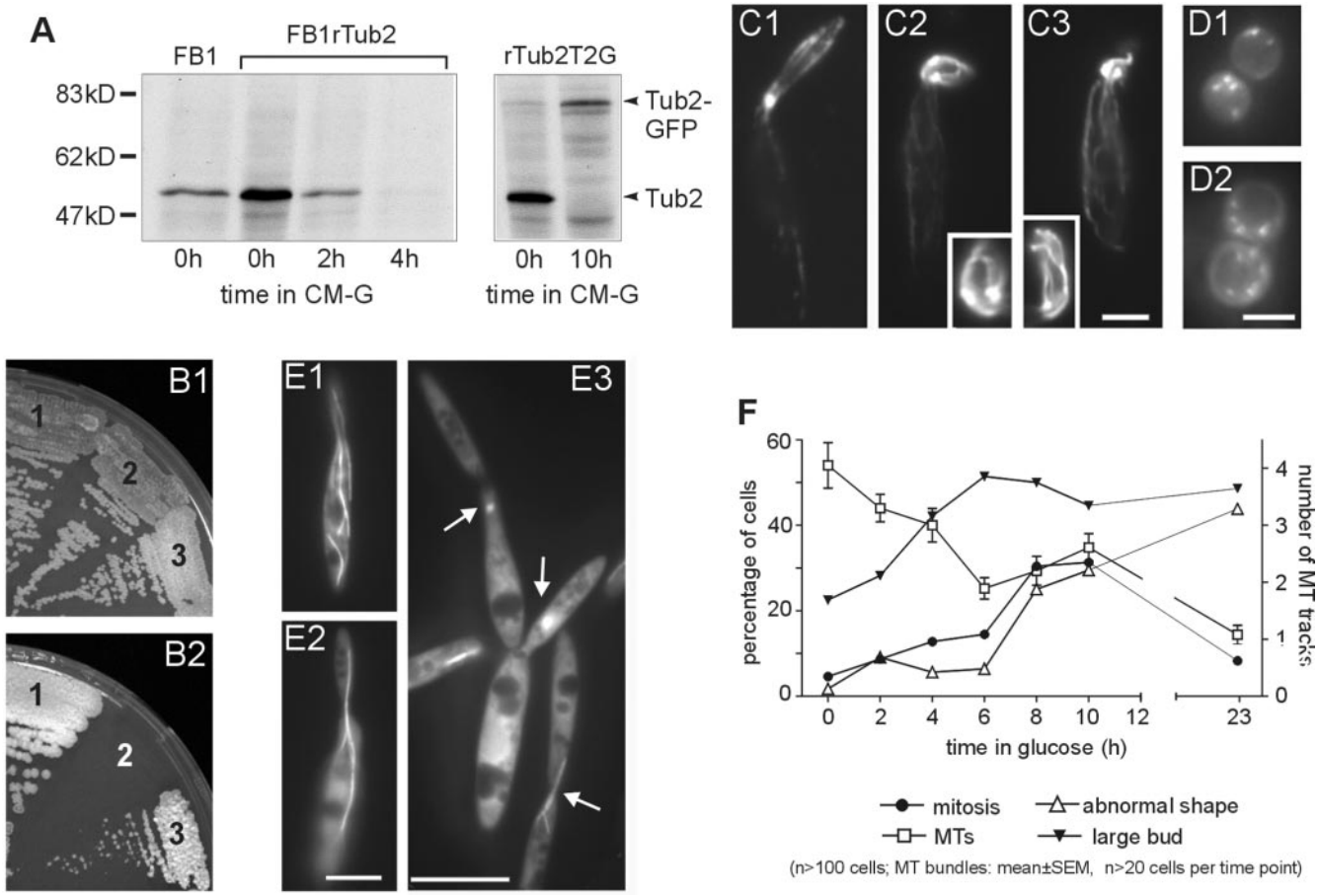

Figure 6. Expression pattern and phenotype of a conditional Tub2 mutant. (A) Tub2 and Tub2-GFP was detected using G9 antibody in wild-type strain FB1 and mutants FB1rTub2 and FB1rTub2T2G. Tub2 is about twofold overexpressed in the mutant strains under permissive conditions (CM-A, 0 h) and could be depleted within 4 h in CM-G. Interestingly, Tub2-GFP fusion protein levels increase after growth in CM-G, where *tub2* expression is repressed. (B) Growth of FB1 (1), FB1rTub2 (2), and FB1rTub2T2G (3) on CM-A plates (B1) and CM-G plates (B2). FB1rTub2 does not form colonies on CM-G. This growth defect is partially rescued by the expression of Tub2-GFP in FB1rTub2T2G (B2). (C) Overexpression of Tub2 leads to abnormal PTS that are brighter stained (C2, C3) than in wild-type strain FB1 (C1). Insets provide higher magnification of the PTS region. Bar, 3 μm. (D) Overexpression of Tub2 results in significantly more MT tracks that could be detected in optical cross sections of FB1rTub2GT (D2) compared with FB1GT (D1). Bar, 3 μm. (E) MT organization in strain FB1rTub2GT was relatively normal at permissive conditions (E1). After shift to restrictive conditions, many cells contained less SPB-independent MTs (E2 and E3 after 4 h in CM-G) and large-budded cells accumulated that contained aberrant spindles (arrows in E3). Bars, 3 μm (E1 and E2) and 10 μm (E3). (F) Quantification of the Tub2 depletion phenotype. After shifting FB1rTub2GT to CM-G, cells with abnormal shape slowly accumulated in the culture (left axis), whereas the number of SPB-independent microtubules decreased (right axis). Large-budded cells, which were most likely arrested in mitosis accumulated and remained stationary after 6 h to 24 h (left axis). Correspondingly, the number of cells containing mitotic spindles increased (left axis), until almost all spindle MTs disappeared after 23 h under restrictive conditions.

MTs undergo a rearrangement during budding and this polarization toward the bud coincided with the appearance of two α-tubulin–containing spheres at the growing cell pole. This led to the speculation that these PTS are polar MTOCs that nucleate SPB-independent MTs. Alternatively, interphase MTs might be nucleated at the SPB, released, and subsequently transported toward the bud, and an adequate MT motility was found in *U. maydis* (Steinberg *et al.*, 2001). To get further insight into the mechanism of cell cycle-dependent nucleation and reorientation of MTs, we marked MT plus-ends by a fusion of the EB1-like protein Peb1 and YFP and followed MT minus-ends by using γ-tubulin-GFP.

Bipolar MT Bundles Are Formed after Random Nucleation in G1 Phase

Bipolar MT bundles traverse the length of the cell during G1 and S phase in *U. maydis*. These MTs were neither anchored nor nucleated at the SPB. Concomitantly, we observed MT nucleations within the cytoplasm by using Peb1-YFP. Benomyl washout experiments revealed the

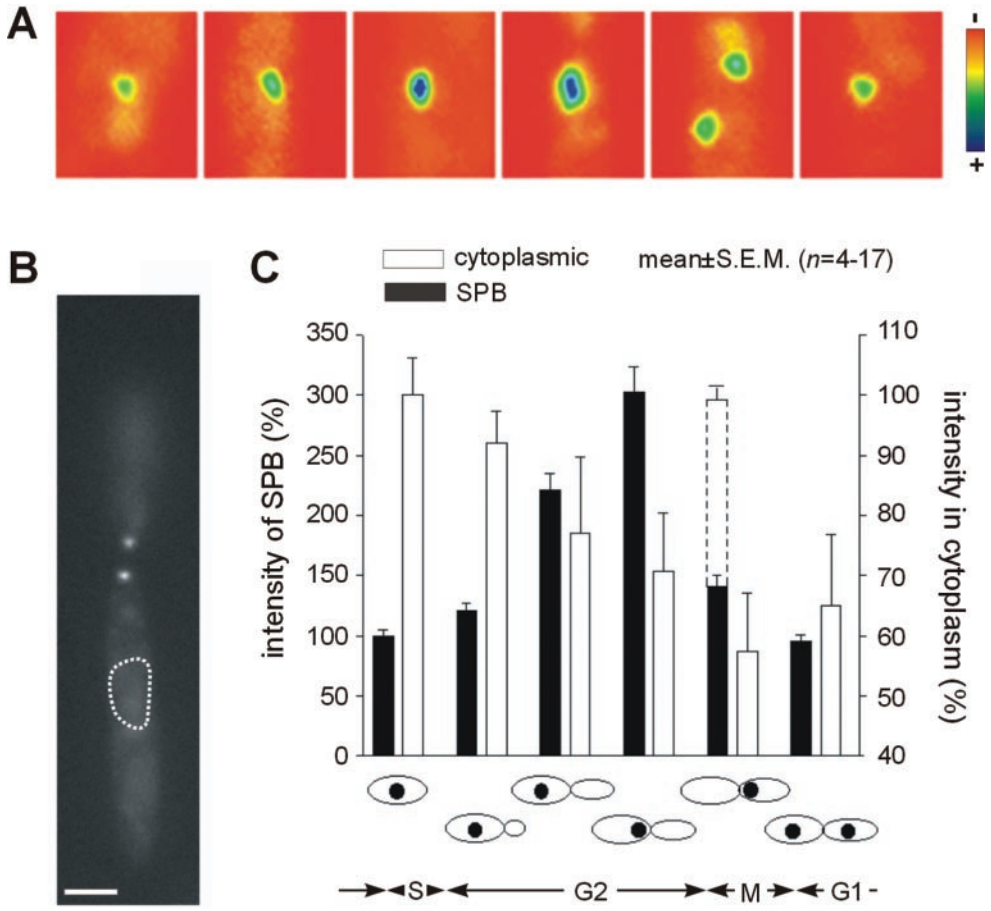

Figure 7. Cytoplasmic pool of Tub2-GFP fusion protein is recruited to the SPB during bud growth. (A) Pseudocolor images of Tub2-GFP fusion protein at the SPB during the cell cycle of FB2T2G. Only weak signals are detected in unbudded cells; however, the Tub2-GFP content gradually increased until SPB separation occurred in mitosis. Note that the images reflect the growth stages depicted in Figure 7C. Signal intensities are expressed in pseudocolors (blue, strong; red, weak). (B) Mitotic cell of FB2rTub2GFP is shown as an example, how cytoplasmic background intensity of Tub2-GFP was measured. Regions comparable with the marked by the dashed line excluded large organelles and the narrow bud neck, and served for estimating the average intensity per pixel. (C) Quantification of Tub2-GFP rearrangement during stages of the cell cycle. Growth and cell cycle stages are given according to (Snetselaar and McCann, 1997). The intensity of Tub2-GFP in SPBs and the cytosol in unbudded cells was set to 100%. The amount of Tub2-GFP bound to the SPB continuously increased during bud growth, remained constant during SPB separation in mitosis (dotted line represents intensity of pairs of SPBs in mitosis), and decreased during G1. The intensity of cytoplasmic Tub2-GFP staining shows the inverse behavior, suggesting a cycling of γ-tubulin between the SPB and the cytoplasm. Values are given as the mean ± SEM for each stage.

existence of numerous nucleation sites, which were randomly distributed within the cytoplasm and often seemed to nucleate more than one MT (Figure 8A). The spontaneous nucleation of single MTs in the cytoplasm of mammalian cells was shown previously (Vorobjev *et al.*, 1997; Yvon and Wadsworth, 1997), and one could argue that benomyl-induced MT disruption leads to an elevated tubulin concentration that may influence nucleating capacity. However, we did not observe cytoplasmic nucleations during benomyl recovery of mitotic cells (our unpublished data) and comparable experiments were done to determine the localization of MTOCs in other cell systems (Meads and Schroer, 1995; Yvon and Wadsworth, 1997; Chabin-Brion *et al.*, 2001; Tran *et al.*, 2001; Vorobjev *et al.*, 2001). In addition, we show herein that the cytoplasmic γ-tubulin pool reaches its peak level in G1/S phase and demonstrate that depletion of γ-tubulin leads to a significant decrease in the number of free MTs. This implies a role for γ-tubulin in nucleation at the cytoplasmic MT nucleating centers, although it was impossible to localize γ-tubulin at theses MTOCs due to its cytoplasmic background. Interestingly, these sites seem to be responsible for MT nucleation, but do not organize these MTs. Immediately after benomyl treatment individual MTs were observed, but they were rapidly gathered into three to four bundles, demonstrating the capability of the cytoplasm to organize randomly nucleated MTs into bundles. At present, the mechanism that underlies this phenomenon is unknown. The MT cytoskeleton of *U. maydis* is exceptionally motile, showing bending, sliding, and motion along

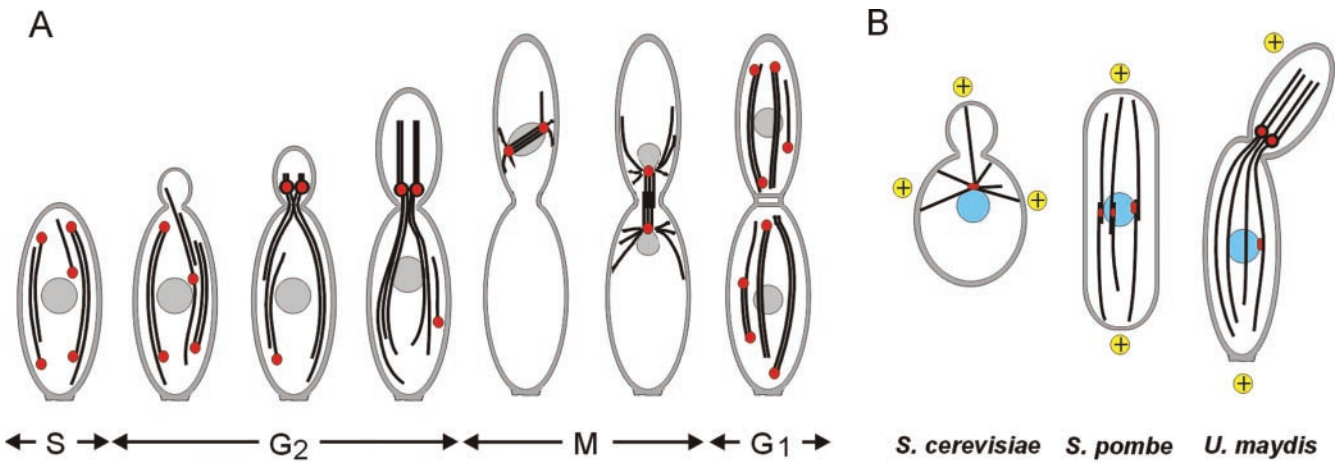

Figure 8. Schematic drawing of MT organization during the cell cycle of *U. maydis* and in different yeast-like cells during interphase. (A) MT bundles span the whole length of the *U. maydis* cell and contain antipolar-oriented MTs during G1 and S phase. These MTs are nucleated at cytoplasmic-nucleating centers. A polarization of the MT cytoskeleton occurs in G2 when the bud reaches ~15% of mother cell length, because MTs are nucleated and anchored at a polar MTOC in the bud neck region. At onset of mitosis, the SPBs start to nucleate MTs, which form the spindle and asters. Sites of MT nucleation are drawn in red, nuclei in gray, MTs in black. Cell cycle stages indicated below. (B) In *S. cerevisiae* interphase MTs emanate from the SPB with their plus ends pointing to the cortex (Barnes *et al.*, 1990). The interphase MT cytoskeleton of *S. pombe* is organized from multiple MTOCs on or near the nucleus, whereas the SPB is inactive (Masuda *et al.*, 1992; Tran *et al.*, 2001). The MT plus-ends grow toward both cell poles and position the nucleus in the cell center by the balanced pushing against the cortex of both cell poles (Tran *et al.*, 2001). MT organization in *U. maydis* in G2 phase is characterized by a polar MTOC near the bud neck, which organizes the minus ends at the neck, whereas MT plus-ends reach out into the bud and the mother cell. The SPB is inactive during interphase. Nuclei are drawn in light blue, and MTs are in black and MTOCs in red. MT plus-ends are indicated by a yellow highlighted plus sign.

the cortex (Steinberg *et al.*, 2001). This argues for an unknown motor activity that might arrange MTs into bundles, thereby participating in MT organization in this fungus.

A Polar MTOC Organizes Unipolar MT Bundles during G2

A striking MT reorganization occurred during early bud growth. This was characterized by MT nucleation events at the PTS region, which seems to display all the necessary features of a noncentrosomal MTOC (Figure 8A). This includes promotion of MT nucleation, organization of MTs, thereby generating organized MT patterns, and a cell cycle dependency of its activity. In addition, we detected essential factors for MT nucleation and anchoring in the PTS region. This includes γ-tubulin, which is known to nucleate MTs at centrosomes as well as at other MTOCs (Oakley, 2000). Although the presence of an MPM-2–reactive epitope does not unequivocally demonstrate that an MTOC is indeed nucleating MTs (Masuda *et al.*, 1992; Martin *et al.*, 1997), the functional importance of MPM-2 detectable phosphoproteins for MT nucleation had clearly been demonstrated in various systems (Centonze and Borisy, 1990; Masuda *et al.*, 1992; Felix *et al.*, 1994). Furthermore, cells with lateral buds contain heavily bent MTs that emanate from PTS and reach into the mother cell. Bending of MTs requires force (Felgner *et al.*, 1996), and we consider it unlikely that MTs reach the lateral growth region by a chance mechanism. Therefore, we take this observation as another indication for polar MT nucleation at the PTS region.

Previous studies have shown that the spherical tubulin structures assemble before bud formation (Steinberg *et al.*, 2001), suggesting that budding coincides with polar MT nucleation. However, the data presented herein demonstrate that polar MT nucleation did not become predominant before the bud reached 15% of mother cell length and small lateral buds did not contain MTs. Therefore, it seems that the PTS assemble long before they become an active MTOC. At present it is unclear how the PTS are formed at the polar growth region. One potential candidate that might support the assembly of the PTS is actin because it was shown to be essential for a comparable process, the formation of the equatorial MTOC during anaphase B in *S. pombe* (Heitz *et al.*, 2001). In addition, dynein-dependent transport might play a role, as the PTS lose their polar localization in dynein mutants (Straube *et al.*, 2001). Thus, elucidating the mechanism of PTS assembly at the growing cell pole will be of key importance for the understanding of MT polarization during budding in *U. maydis.*

γ-Tubulin Cycles between SPB and Cytoplasmic Pool

We demonstrate herein for the first time that a fungal γ-tubulin is gradually recruited to the SPB during bud growth, whereas its cytoplasmic pool decreases in a reciprocal manner. A comparable recruitment of γ-tubulin to the centrosome was observed in mammalian cells, but in contrast to *U. maydis*, this occurred exclusively during prophase and the amount of centrosome-associated γ-tubulin decreased in anaphase and remained constant during interphase (Khodja-

kov and Rieder, 1999). However, although variations exist, the phenomenon of γ-tubulin cycling seems to be conserved from mammals to fungi. Possible roles for γ-tubulin in the cytoplasm could be MT nucleation from noncentrosomal sites as seen in *U. maydis* during interphase or as reported previously in animal and fungal cells (Yvon and Wadsworth, 1997; Chabin-Brion *et al.*, 2001; Heitz *et al.*, 2001). It could also serve as a minus-end cap of released or broken MTs, thereby preventing their minus-end depolymerization (Wiese and Zheng, 2000) or might modify MT plus-end dynamics (Paluh *et al.*, 2000; Vogel *et al.*, 2001).

γ-Tubulin concentration at the SPBs reaches its peak level at onset of mitosis, when the duplicated SPBs become active and nucleate spindle and astral MTs, suggesting that increasing amounts of γ-tubulin support MT formation (Figure 8A). However, it is unlikely that the recruitment of a certain amount of γ-tubulin is sufficient for SPB activation. It was shown for fission yeast that the phosphorylation of SPB components is necessary to switch MT-nucleating activity on (Masuda *et al.*, 1992). Phosphoepitopes were detected at the polar MTOC and the mitotic SPB of *U. maydis*, indicating that unknown kinases participate in the activation of these MTOCs. Cells containing a mitotic nucleus never showed non-SPB MT nucleation even after recovery from benomyl treatment (our unpublished data), suggesting that the capacity to nucleate MTs at cytoplasmic sites is repressed in M phase. Exactly the same occurs in vertebrates when centrosome-dependent nucleation continues, whereas noncentrosomal nucleation is shut off during mitosis (Verde *et al.*, 1990). This implies that a conserved mechanism may exist in animals and fungi, whereby MT nucleation is under control of the cell cycle. Interestingly, in budding cells the polar MTOC is dominant but nucleation at other sites is not completely repressed. This is most obvious from the facts that ~15% of all polymerizations were still directed toward the PTS and that benomyl treatment of cells in G2 revealed active nucleation sites in the mother cell (our unpublished data). This raises the question of whether the mechanisms of activation and repression of MT nucleation during G2 and M phase are similar. Not much is known about these mechanisms, and it will be a fascinating project for the future to elucidate the involved components.

MTOCs at Bud Neck Ensure That MTs Reach Growth Region

MTs are polar and stiff structures that are usually nucleated at the central nucleus and reach the growth region by elongation at their plus ends (Desai and Mitchison, 1997). This principle of MT organization was described for the yeast *S. cerevisiae* (Figure 8B), where MTs search for the bud tip by a stochastic chance mechanism that enables proper spindle positioning (Korinek *et al.*, 2000; Lee *et al.*, 2000). Another well known example is the fission yeast *S. pombe* (Figure 8B), where MTs are nucleated and stabilized by numerous MTOCs on the nuclear surface and polymerization takes their plus ends to the cell poles (Tran *et al.*, 2001), thereby ensuring that MT based delivery of growth components reaches the growing cell poles (Hayles and Nurse, 2001). In this study, we describe an alternative principle of how a cell ascertains that MTs reach the growth region. In *U. maydis*, MT nucleation occurs distantly from the nucleus at a polar MTOC near the bud neck, which organizes MTs where they are needed. This results in a polarized MT cytoskeleton and allows minus-end–directed MT-based transport toward the growth region (Figure 8B). The establishment of polar MTOCs allows MT organization independent of cell shape and might be important due to the elongated cell shape and the distinct budding angle (34 ± 17°, n = 33 cells), which makes it unlikely that MTs reach the bud tip by a chance mechanism as it happens in budding yeast. Furthermore, *U. maydis* is a dimorphic fungus, which undergoes complex developmental changes during its life cycle, and this may necessitate an enhanced ability to organize its MT cytoskeleton in a highly flexible manner.

ACKNOWLEDGMENTS

We thank Dr. E. Kube-Granderath for initial help in identifying *tub2*; I. Schulz, M. Artmeier, and Dr. R. Wedlich-Söldner for technical support; and Dr. A. Neumeyer-Heidenthal from (Visitron Systems, Munich, Germany) for supplying devices and technical expertise to do deconvolution microscopy. The Bayer CropScience AG is acknowledged for providing the genomic sequence of *Umpeb1*. We are grateful to Dr. Gagan Gupta for critical reading of the manuscript and to Dr. R. Kahmann for generous support. The work was supported by the Deutsche Forschungsgemeinschaft SFB 413 and SP 1111. B.R.O. is supported by grants from the National Institute of General Medical Science and the National Science Foundation.

REFERENCES

Banuett, F. (1995). Genetics of *Ustilago maydis*, a fungal pathogen that induces tumors in maize. Annu. Rev. Genet. *29*, 179–208.

Banuett, F., and Herskowitz, I. (1989). Different a alleles of *Ustilago maydis* are necessary for maintenance of filamentous growth but not for meiosis. Proc. Natl. Acad. Sci. USA *86*, 5878–5882.

Barnes, G., Drubin, D.G., and Stearns, T. (1990). The cytoskeleton of *Saccharomyces cerevisiae*. Curr. Opin. Cell Biol. *2*, 109–115.

Beinhauer, J.D., Hagan, I.M., Hegemann, J.H., and Fleig, U. (1997). Mal3, the fission yeast homologue of the human APC-interacting protein EB-1 is required for microtubule integrity and the maintenance of cell form. J. Cell Biol. *139*, 717–728.

Berrueta, L., Kraeft, S.K., Tirnauer, J.S., Schuyler, S.C., Chen, L.B., Hill, D.E., Pellman, D., and Bierer, B.E. (1998). The adenomatous polyposis coli-binding protein EB1 is associated with cytoplasmic and spindle microtubules. Proc. Natl. Acad. Sci. USA *95*, 10596–10601.

Bottin, A., Kämper, J., and Kahmann, R. (1996). Isolation of a carbon source-regulated gene from *Ustilago maydis*. Mol. Gen. Genet. *253*, 342–352.

Centonze, V.E., and Borisy, G.G. (1990). Nucleation of microtubules from mitotic centrosomes is modulated by a phosphorylated epitope. J. Cell Sci. *95*, 405–411.

Chabin-Brion, K., Marceiller, J., Perez, F., Settegrana, C., Drechou, A., Durand, G., and Pous, C. (2001). The Golgi complex is a microtubule-organizing organelle. Mol. Biol. Cell *12*, 2047–2060.

Davis, F.M., Tsao, T.Y., Fowler, S.K., and Rao, P.N. (1983). Monoclonal antibodies to mitotic cells. Proc. Natl. Acad. Sci. USA *80*, 2926–2930.

Desai, A., and Mitchison, T.J. (1997). Microtubule polymerization dynamics. Annu. Rev. Cell. Dev. Biol. *13*, 83–117.

Felgner, H., Frank, R., and Schliwa, M. (1996). Flexural rigidity of microtubules measured with the use of optical tweezers. J. Cell Sci. *109*, 509–516.

Felix, M.A., Antony, C., Wright, M., and Maro, B. (1994). Centrosome assembly in vitro: role of γ-tubulin recruitment in *Xenopus* sperm aster formation. J. Cell Biol. *124*, 19–31.

Hagan, I.M. (1998). The fission yeast microtubule cytoskeleton. J. Cell Sci. *111*, 1603–1612.

Hayles, J., and Nurse, P. (2001). A journey into space. Nat. Rev. Mol. Cell. Biol. *2*, 647–656.

Heath, I.B. (1981). Nucleus associated organelles of fungi. Int. Rev. Cytol. *69*, 191–221.

Heitz, M.J., Petersen, J., Valovin, S., and Hagan, I.M. (2001). MTOC formation during mitotic exit in fission yeast. J. Cell Sci. *114*, 4521–4532.

Holliday, R. (1974). *Ustilago maydis*. In: Handbook of Genetics, ed. R.C. King, New York: Plenum Press.

Horio, T., Basaki, A., Takeoka, A., and Yamato, M. (1999). Lethal level overexpression of γ-tubulin in fission yeast causes mitotic arrest. Cell Motil. Cytoskeleton *44*, 284–295.

Horio, T., Uzawa, S., Jung, M.K., Oakley, B.R., Tanaka, K., and Yanagida, M. (1991). The fission yeast γ-tubulin is essential for mitosis and is localized at microtubule organizing centers. J. Cell Sci. *99*, 693–700.

Hyman, A., and Karsenti, E. (1998). The role of nucleation in patterning microtubule networks. J. Cell Sci. *111*, 2077–2083.

Joshi, H.C. (1994). Microtubule organizing centers and γ-tubulin. Curr. Opin. Cell Biol. *6*, 54–62.

Joshi, H.C., Palacios, M.J., McNamara, L., and Cleveland, D.W. (1992). Gamma-tubulin is a centrosomal protein required for cell cycle-dependent microtubule nucleation. Nature *356*, 80–83.

Keating, T.J., Peloquin, J.G., Rodionov, V.I., Momcilovic, D., and Borisy, G.G. (1997). Microtubule release from the centrosome. Proc. Natl. Acad. Sci. USA *94*, 5078–5083.

Keon, J.P., White, G.A., and Hargreaves, J.A. (1991). Isolation, characterization and sequence of a gene conferring resistance to the systemic fungicide carboxin from the maize smut pathogen *Ustilago maydis*. Curr. Genet. *19*, 475–481.

Khodjakov, A., and Rieder, C.L. (1999). The sudden recruitment of γ-tubulin to the centrosome at the onset of mitosis and its dynamic exchange throughout the cell cycle, do not require microtubules. J. Cell Biol. *146*, 585–596.

Kirschner, M.W. (1978). Microtubule assembly and nucleation. Int. Rev. Cytol. *54*, 1–71.

Korinek, W.S., Copeland, M.J., Chaudhuri, A., and Chant, J. (2000). Molecular linkage underlying microtubule orientation toward cortical sites in yeast. Science *287*, 2257–2259.

Kube-Granderath, E., and Schliwa, M. (1997). Unusual distribution of γ-tubulin in the giant fresh water amoeba *Reticulomyxa filosa*. Eur. J. Cell Biol. *72*, 287–296.

Kumar, S., Tamura, K., Jakobsen, I.B., and Nei, M. (2001). MEGA2: molecular evolutionary genetics analysis software. Bioinformatics *17*, 1244–1245.

Lee, L., Tirnauer, J.S., Li, J., Schuyler, S.C., Liu, J.Y., and Pellman, D. (2000). Positioning of the mitotic spindle by a cortical-microtubule capture mechanism. Science *287*, 2260–2262.

Leguy, R., Melki, R., Pantaloni, D., and Carlier, M.F. (2000). Monomeric γ-tubulin nucleates microtubules. J. Biol. Chem. *275*, 21975–21980.

Lupas, A., Van Dyke, M., and Stock, J. (1991). Predicting coiled coils from protein sequences. Science *252*, 1162–1164.

Martin, M.A., Osmani, S.A., and Oakley, B.R. (1997). The role of γ-tubulin in mitotic spindle formation and cell cycle progression in *Aspergillus nidulans*. J. Cell Sci. *110*, 623–633.

Masuda, H., Sevik, M., and Cande, W.Z. (1992). In vitro microtubule-nucleating activity of spindle pole bodies in fission yeast *Schizosaccharomyces pombe*: cell cycle-dependent activation in xenopus cell-free extracts. J. Cell Biol. *117*, 1055–1066.

McDonald, A.R., Liu, B., Joshi, H.C., and Palevitz, B.A. (1993). Gamma-tubulin is associated with a cortical-microtubule-organizing zone in the developing guard cells of *Allium cepa* L. Planta *191*, 357–361.

Meads, T., and Schroer, T.A. (1995). Polarity and nucleation of microtubules in polarized epithelial cells. Cell Motil. Cytoskeleton *32*, 273–288.

Mimori-Kiyosue, Y., Shiina, N., and Tsukita, S. (2000). The dynamic behavior of the APC-binding protein EB1 on the distal ends of microtubules. Curr. Biol. *10*, 865–868.

Morrison, E.E., Wardleworth, B.N., Askham, J.M., Markham, A.F., and Meredith, D.M. (1998). EB1, a protein which interacts with the APC tumor suppressor, is associated with the microtubule cytoskeleton throughout the cell cycle. Oncogene *17*, 3471–3477.

Muresan, V., Joshi, H.C., and Besharse, J.C. (1993). Gamma-tubulin in differentiated cell types: localization in the vicinity of basal bodies in retinal photoreceptors and ciliated epithelia. J. Cell Sci. *104*, 1229–1237.

Nabi, I.R. (1999). The polarization of the motile cell. J. Cell Sci. *112*, 1803–1811.

Oakley, B.R. (2000). An abundance of tubulins. Trends Cell Biol. *10*, 537–542.

Oakley, C.E., and Oakley, B.R. (1989). Identification of γ-tubulin, a new member of the tubulin superfamily encoded by *mipA* gene of *Aspergillus nidulans*. Nature *338*, 662–664.

Oakley, B.R., Oakley, C.E., Yoon, Y., and Jung, M.K. (1990). Gamma-tubulin is a component of the spindle pole body that is essential for microtubule function in *Aspergillus nidulans*. Cell *61*, 1289–1301.

Ovechkina, Y., and Oakley, B.R. (2001). Gamma tubulin in plant cells. Methods Cell Biol. *67*, 195–212.

Paluh, J.L., Nogales, E., Oakley, B.R., McDonald, K., Pidoux, A.L., and Cande, W.Z. (2000). A mutation in γ-tubulin alters microtubule dynamics and organization and is synthetically lethal with the kinesin-like protein pkl1p. Mol. Biol. Cell *11*, 1225–1239.

Sambrooke, J., Fritsch, E.F., and Maniatis, T. (1989). Molecular Cloning: A Laboratory Manual, Cold Spring Harbor, NY: Cold Spring Harbor Laboratory.

Schulz, B., Banuett, F., Dahl, M., Schlesinger, R., Schaefer, W., Martin, T., Herskowitz, I., and Kahmann, R. (1990). The B alleles of *Ustilago maydis* whose combinations program pathogenic development code for polypeptides containing a homeodomain-related motif. Cell *60*, 295–306.

Snetselaar, K.M., and McCann, M.P. (1997). Using microdensitometry to correlate cell morphology with the nuclear cycle in *Ustilago maydis*. Mycologia *89*, 689–697.

Spellig, T., Bottin, A., and Kahmann, R. (1996). Green fluorescent protein (GFP) as a new vital marker in the phytopathogenic fungus *Ustilago maydis*. Mol. Gen. Genet. *252*, 503–509.

Steinberg, G., Wedlich-Soldner, R., Brill, M., and Schulz, I. (2001). Microtubules in the fungal pathogen *Ustilago maydis* are highly dynamic and determine cell polarity. J. Cell Sci. *114*, 609–622.

Straube, A., Enard, W., Berner, A., Wedlich-Soldner, R., Kahmann, R., and Steinberg, G. (2001). A split motor domain in a cytoplasmic dynein. EMBO J. *20*, 5091–5100.

Thompson, J.D., Gibson, T.J., Plewniak, F., Jeanmougin, F., and Higgins, D.G. (1997). The CLUSTALX windows interface: flexible strategies for multiple sequence alignment aided by quality analysis tools. Nucleic Acids Res. *25*, 4876–4882.

Tirnauer, J.S., and Bierer, B.E. (2000). EB1 proteins regulate microtubule dynamics, cell polarity, and chromosome stability. J. Cell Biol. *149*, 761–766.

Tirnauer, J.S., O'Toole, E., Berrueta, L., Bierer, B.E., and Pellman, D. (1999). Yeast Bim1p promotes the G1-specific dynamics of microtubules. J. Cell Biol. *145*, 993–1007.

Tran, P.T., Marsh, L., Doye, V., Inoue, S., and Chang, F. (2001). A mechanism for nuclear positioning in fission yeast based on microtubule pushing. J. Cell Biol. *153*, 397–411.

Vaughn, K.C., and Harper, J.D. (1998). Microtubule-organizing centers and nucleating sites in land plants. Int. Rev. Cytol. *181*, 75–149.

Verde, F., Labbe, J.C., Doree, M., and Karsenti, E. (1990). Regulation of microtubule dynamics by Cdc2 protein kinase in cell-free extracts of *Xenopus* eggs. Nature *343*, 233–238.

Vogel, J., Drapkin, B., Oomen, J., Beach, D., Bloom, K., and Snyder, M. (2001). Phosphorylation of γ-tubulin regulates microtubule organization in budding yeast. Dev. Cell *1*, 621–631.

Vorobjev, I., Malikov, V., and Rodionov, V. (2001). Self-organization of a radial microtubule array by dynein-dependent nucleation of microtubules. Proc. Natl. Acad. Sci. USA *98*, 10160–10165.

Vorobjev, I.A., Svitkina, T.M., and Borisy, G.G. (1997). Cytoplasmic assembly of microtubules in cultured cells. J. Cell Sci. *110*, 2635–2645.

Waterman-Storer, C.M., and Salmon, E.D. (1997). Actomyosin-based retrograde flow of microtubules in the lamella of migrating epithelial cells influences microtubule dynamic instability and turnover and is associated with microtubule breakage and treadmilling. J. Cell Biol. *139*, 417–434.

Wedlich-Soldner, R., Bolker, M., Kahmann, R., and Steinberg, G. (2000). A putative endosomal t-SNARE links exo- and endocytosis in the phytopathogenic fungus *Ustilago maydis*. EMBO J. *19*, 1974–1986.

Wedlich-Soldner, R., Straube, A., Friedrich, M.W., and Steinberg, G. (2002). A balance of KIF1A-like kinesin and dynein organizes early endosomes in the fungus *Ustilago maydis*. EMBO J. *21*, 2946–2957.

Wiese, C., and Zheng, Y. (2000). A new function for the γ-tubulin ring complex as a microtubule minus-end cap. Nat. Cell Biol. *2*, 358–364.

Yvon, A.M., and Wadsworth, P. (1997). Non-centrosomal microtubule formation and measurement of minus end microtubule dynamics in A498 cells. J. Cell Sci. *110*, 2391–2401.